SnO₂/Graphene Nanoplatelet Nanocomposites: Solid-State Method Synthesis With High Ethanol Gas-Sensing Performance

Run Zhang [1,2], Jian-Bo Jia [1,2]*, Jian-Liang Cao [1,2] and Yan Wang [1,3]*

[1] The Collaboration Innovation Center of Coal Safety Production of Henan Province, Henan Polytechnic University, Jiaozuo, China, [2] Department of Chemical Engineering and Technology, College of Chemistry and Chemical Engineering, Henan Polytechnic University, Jiaozuo, China, [3] School of Safety Science and Engineering, State Key Laboratory Cultivation Base for Gas Geology and Gas Control, Henan Polytechnic University, Jiaozuo, China

INTRODUCTION

Graphene nanoplatelet (GNP) is a well-known 2D carbon nanomaterial composed of network structure of sp^2-hybridized carbon atoms. So far, two main strategies (exfoliation and chemical oxidation-reduction) have been used for the preparation of GNP from graphite. Unfortunately, a lot of defects are caused by the strong oxidizing reagents on the GNP produced by chemical oxidation-reduction method, and such GNP lost the remarkable electrical and mechanical properties (Coleman, 2013). Exfoliation method could be adopted to product high-quality GNP from graphite, but the yield of GNP is quite low (∼1 wt.%) (Hernandez et al., 2008). Hence, the requisite large scale production of high-quality GNP remains a challenging task.

Even so, GNP is expected as a promising material for gas sensing due to its unrivaled physiochemical and electronic properties such as excellent flexibility, large specific surface area and high conductivity. Nevertheless, owing to the poor gas-sensing selectivity, GNP exhibited responses to several kinds of gas (Yoon et al., 2012; Nemade and Waghuley, 2013). But when GNP was incorporated with other sensor materials, like metal oxide semiconductors (MOSs), it could remarkably improve the sensing performance of the sensor materials (Eom et al., 2017; Thu et al., 2018). The MOSs phase facilitates the adsorption/desorption process of tested gas, thereby activating the reactions occurring on the carbon surface, which in turn increases the response speed and response/recovery time. In addition, n-p junctions can be formed by GNP with n-type metal oxides, and the resulting novel nanostructures perform much better gas sensing performance than single materials (Neri et al., 2013).

As an n-type metal oxide semiconductor, tin dioxide (SnO_2) has a wide band gap of Eg = 3.6 eV and excellent optical and electrical properties. SnO_2 have been one of the most extensive studied materials due to its wide applications including in transparent conductive electrodes and transistors (Liu et al., 2018; Satoh et al., 2018), lithium-ion batteries (Zhao et al., 2016; Shi et al., 2017), dye-sensitized solar cells (Hagfeldt et al., 2010), photocatalysis (Aslam et al., 2018; Praus et al., 2018) and gas sensors (Narjinary et al., 2017; Long et al., 2018; Xu et al., 2018). For gas sensing application, SnO_2 and SnO_2 based composites also show admirable gas sensing properties like low-cost, low detection limit, fast response and recovery, high response and good stability (Yan et al., 2015; Cao et al., 2017; Kim et al., 2017).

Herein, we put forward a simple and potentially scalable method to obtaining massive high-quality GNP from exfoliation of flake graphite in K_2FeO_4/H_2SO_4, and use the solid-state method to synthesize SnO_2 decorated graphene nanoplatelet nanocomposites

(SnO$_2$/GNP) with different mass ratio of SnO$_2$ and GNP. The as-prepared SnO$_2$/GNP nanocomposites possess the two-dimensional (2D) structure, and the 2D GNP accelerating the preferential growth and preventing the agglomeration of the SnO$_2$ nanoparticles. The gas sensing tests indicated that the sensors based on GNP/SnO$_2$ nanocomposites possess high sensitivity and excellent characteristic of response and recovery toward ethanol vapor. The sensor response was found to be dependent on the mass ratio of GNP in the composites and it reaches the maximum response when the mass percentage of GNP in the composites is 5%.

EXPERIMENTAL

Preparation of the GNP/SnO$_2$ Nanocomposites

All the reagents were of analytical grade (AR) and used as received without further purification. The preparation of GNP was listed in the **Supplementary Material**. A typical synthesis process of GNP/SnO$_2$ nanocomposites with 5 wt.% GNP content can be described as follows: 7 g of SnCl$_4$·5H$_2$O, 0.15 g of GNP and 6 ml of PEG-400 were mixed adequately and ground together in an agate mortar. Subsequently, 3.2 g of NaOH was slowly added to the mixtures and ground together for about 30 min. The reaction started readily during the addition process of NaOH, accompanied by release of heat. As the reaction proceeded, the mixture became mushy. Then samples were collected, washed several times with distilled water and absolute

ethanol, and dried at 60°C overnight in a drying oven. Finally, the product was ground to powder, marked as GNP/SnO$_2$-5. 2.5 and 7.5 wt.% GNP of GNP/SnO$_2$ nanocomposites were prepared using the aforementioned method, and marked as GNP/SnO$_2$-2.5 and GNP/SnO$_2$-7.5, respectively. For comparison, the same method was used to synthesize SnO$_2$ nanoparticles without GNP.

The characterization, sensor fabrication and measurement (**Figure S1**) were listed in the Supplementary Material.

RESULTS AND DISCUSSION

The XRD diffraction pattern of GNP is almost identical to that of pristine graphite (**Figure 1A**), revealing that no structural change occurred during the exfoliating process. The intensity of (002) peak centered at 26.5° of GNP decreases obviously compared with that of pristine graphite due to the ultrathin thickness of GNP (Zhang et al., 2016). The XRD diffraction patterns of pure SnO$_2$ nanoparticles and GNP/SnO$_2$ nanocomposites are shown in **Figure 1B**. We can see that four distinct diffraction peaks of SnO$_2$ centered at 2θ of 26.6°, 33.9°, 51.7°, and 65.9°, which are corresponding to the reflection from the (110), (101), (211), and (301) planes of the tetragonal rutile SnO$_2$ (JCPDS Card No. 41-1445), respectively. This confirmed that the synthesis method that SnO$_2$ was successfully prepared by solid-state reaction is feasible and complete. However, as seen from **Figure 1B**, there are no diffraction peak around 26.6° of SnO$_2$ observed in the curves, because the diffraction peaks of 26.5° of GNP is so high that the peak around 26.6° of SnO$_2$ is covered.

FIGURE 1 | (A) XRD patterns of pristine graphite and GNP. **(B)** XRD patterns of SnO$_2$ and the SnO$_2$/GNP nanocomposites with different GNP contents. **(C,D)** TEM and HRTEM images of the SnO$_2$/GNP-5 nanocomposite. **(E)** TG-DSC profiles of the SnO$_2$/GNP-5 nanocomposites. **(F)** The pore size distribution curves of the SnO$_2$ and SnO$_2$/GNP-5 nanocomposite.
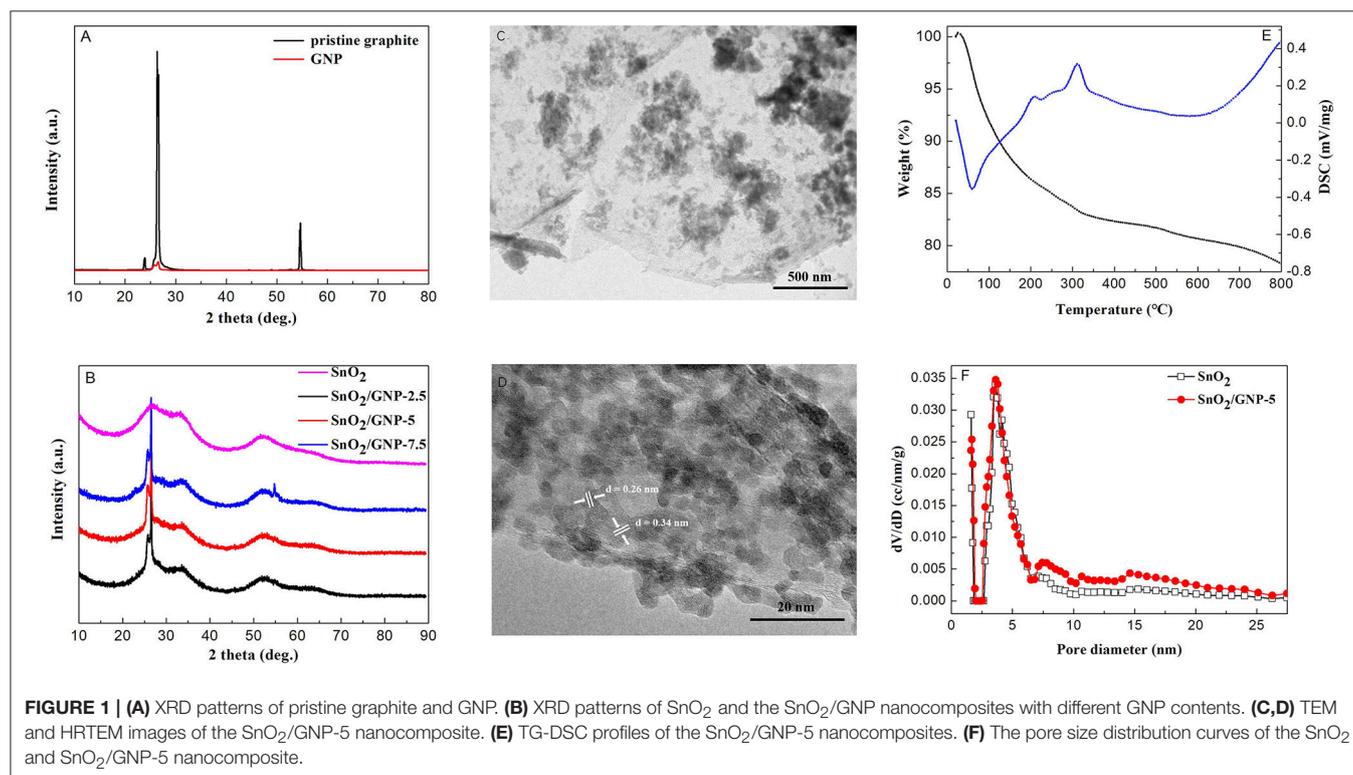
Figure S2a shows the representative FESEM image of pristine graphite. In **Figure S2b** (FESEM image of GNP), two-dimensional (2D) structure of the thin layers can be seen clearly. As shown in **Figure S2c**, the FESEM image of the pure SnO$_2$ exhibits particles with the size of 100–200 nm. The FESEM and TEM images of the GNP/SnO$_2$-5 nanocomposite are presented in **Figure S2d** and **Figure 1C**, respectively, and which show that numerous particles are dispersed on the surface of 2D sheets of GNP. Meanwhile, as can be seen from **Figure 1D**, two phases of GNP and SnO$_2$ are clearly observed and closely in contact to form an intimate interface. And, the lattice fringes with interplanar spacings of 0.26 nm and 0.34 nm can be corresponding to the (101) and (110) planes of SnO$_2$ nanoparticles. It can be concluded that the GNP/SnO$_2$ composites were synthesized successfully using the solid-state method.

TG-DSC analysis revealed the weight change situation of GNP/SnO$_2$-5 nanocomposites from room temperature to 800°C with the heating rate of 10°·min^{-1}. As is shown in **Figure 1E**, there are two stages of weight loss in the TG curve according to the peaks of DSC curve. The first stage in temperature before 300°C is due to desorption of moisture and solvent. The second stage of weight loss is due to the combustion of GNP in air. This result proves that the GNP/SnO$_2$-5 nanocomposite was not decomposed at the operating temperature of 280°C in the procedure of measuring gas-sensing properties.

Figure 1F displays the pore diameter distribution of the SnO$_2$ and GNP/SnO$_2$-5 samples. It can be clearly seen that the pore diameters of pure SnO$_2$ and GNP/SnO$_2$-5 are relatively small, which both the majority concentrate on about 2 nm and 4 nm. The specific surface areas of GNP/SnO$_2$-5 sample is 167.01 m^2·g^{-1}, which is higher than SnO$_2$ (119.67 m^2·g^{-1}). Increasing specific surface area could be in favor of enhancing gas-sensing properties.

Figure 2A shows the response values of pure SnO$_2$ nanoparticles-based sensor and GNP/SnO$_2$-based sensors to 500 ppm of ethanol at different temperatures. From the curves of GNP/SnO$_2$-2.5, GNP/SnO$_2$-5, and GNP/SnO$_2$-7.5, it can be clearly observed that the response values increased with the increase of the temperature. However, the response values decrease when the temperature is above 280°C. As a result, the best operating temperature of GNP/SnO$_2$-based sensors is 280°C. Similarly, the best operating temperature of pure SnO$_2$ sensors is 300°C. We can get a conclusion that the best operating temperature is lowered 20°C because of the joining of GNP. Compared between the different curves, it reaches the maximum response when the mass percentage of GNP in the composites is 5%. The response value of GNP/SnO$_2$-7.5 sample is lower than that of the GNP/SnO$_2$-5 sample. It is because that activation center still focuses on the SnO$_2$ nanoparticle, and the high content of GNP may lead to the decrease of SnO$_2$ nanoparticle on the unit specific surface area. Some SnO$_2$-based materials of ethanol sensing from the literature are summarized in **Table S1**. It can be observed that the GNP/SnO$_2$ composite exhibits superior performances compared with other SnO$_2$-based materials.

Figure S3 displays the response values of sensors based on pure SnO$_2$ and GNP/SnO$_2$-5 to different concentrations of ethanol at 280°C. As shown in the curves, the response values of the two sensors increased with the increasing of ethanol concentrations in the range of 50–2,000 ppm. We can find its regularity through a large number of relevant experiments to establish the relationship between response value and concentration of ethanol. From comparison of two curves, a gradual enhancement in response amplitude was observed for both sensors, and the response amplitudes of GNP/SnO$_2$-5 based sensor are always higher than that of pure SnO$_2$, demonstrating its better sensitivity to ethanol.

It is well known that selectivity is another key criterion for measuring the quality of gas sensors. **Figure 2B** shows the selectivity test results of the pure SnO$_2$ and GNP/SnO$_2$-5 sensors to five different gases of 500 ppm, including methanol, ethanol, methylbenzene, glycerine and methanal. It can be observed that the GNP/SnO$_2$-5-based sensor has good selectivity to ethanol compared to that of pure SnO$_2$ sensor at 280°C. The higher response to ethanol may be because ethanol is more likely to lose electrons in the process of a redox reaction with the absorbed oxygen, and the hydroxyl group (–OH) is much easier to oxidize at the optimum operating temperature.

FIGURE 2 | (A) The response values of SnO$_2$, SnO$_2$/GNP-2.5, SnO$_2$/GNP-5, and SnO$_2$/GNP-7.5 sensors toward 500 ppm of ethanol at different working temperatures. **(B)** The responses of sensors (SnO$_2$ and SnO$_2$/GNP-5) operated at 280°C in 500 ppm of different gases. **(C)** The response-recovery curve of SnO$_2$ and SnO$_2$/GNP-5 toward 500 ppm of ethanol at 280°C.
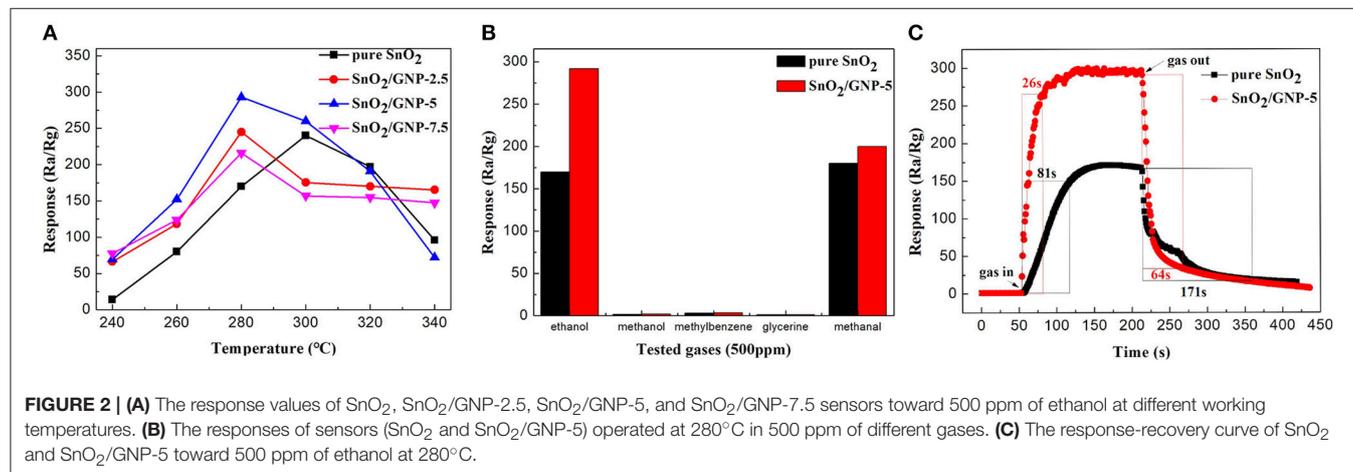
The response–recovery time curve of GNP/SnO$_2$-5-based sensor to 500 ppm of ethanol is shown in **Figure 2C**. Response and recovery time are defined as change in the resistances from Ra to [Ra−90% × (Ra − Rg)] for gas-in and [Ra + 90% × (Ra − Rg)] to gas-out, respectively (Zhang S.S. et al., 2018; Zhang Y.J. et al., 2018). It can be clearly observed that the response increased and decreased quickly when the GNP/SnO$_2$-5-based sensor was exposed to and separated from ethanol, respectively. The response time and the recovery time of GNP/SnO$_2$-5-based sensor are 26 and 64 s, respectively, which are much shorter than of the pure SnO$_2$-based sensor that are 81 and 171 s. The relatively rapid response and recovery time could be due to the unique structure, which is the SnO$_2$ nanoparticles are decorated on the 2D sheet of GNP. This indicates that the large specific surface area is favorable to the adsorption of ethanol, which verifies the above conjecture. **Figure S4** depicts the response values of GNP/SnO$_2$-5-based sensor to 500 ppm of ethanol for every 3 days in 30 days at 280°C, which fall slightly but are maintained around 295. Therefore, the conclusion could be obtained that the GNP/SnO$_2$-5-based gas sensor to ethanol has a satisfactory stability, which confirms that the sensor might have a practical application.

CONCLUSION

In conclusion, we reported an easy method to successfully prepare massive high-quality GNP from exfoliation of flake graphite, and GNP/SnO$_2$ nanocomposites were successfully synthesized by a facile solid-state method. The 2D GNP has no structural change during the exfoliating process from flake graphite, and the SnO$_2$ nanoparticles were highly distributed

on the surface of GNP. The GNP/SnO$_2$ based sensor showed excellent gas sensing performance toward ethanol, and the ameliorative gas-sensing properties may be due to the accrescent specific surface area and the interaction between 2D GNP and SnO$_2$ nanoparticles. Due to the procedure is convenient and environment-friendly, and good gas sensing property of the SnO$_2$/GNP nanocomposite, it could be a promising candidate for ethanol detection.

AUTHOR CONTRIBUTIONS

RZ performed the experiments and analyzed the data with the help from J-LC. J-BJ and YW conceived the study. All authors discussed the results and wrote the manuscript.

FUNDING

SUPPLEMENTARY MATERIAL

The Supplementary Material for this article can be found online at: https://www.frontiersin.org/articles/10.3389/fchem.2018.00337/full#supplementary-material

REFERENCES

Aslam, M., Qamar, M. T., Ali, S., Rehman, A. U., Soomro, M. T., Ahmed, I., et al. (2018). Evaluation of SnO$_2$ for sunlight photocatalytic decontamination of water. *J. Environ. Manage.* 217, 805–814. doi: 10.1016/j.jenvman.2018.04.042

Cao, J., Qin, C., Wang, Y., Zhang, B., Gong, Y., and Zhang, H. L. (2017). Calcination method synthesis of SnO$_2$/g-C$_3$N$_4$ Composites for a high-performance ethanol gas sensing application. *Nanomaterials* 7:98. doi: 10.3390/nano7050098

Coleman, J. N. (2013). Liquid exfoliation of defect-free graphene. *Acc. Chem. Res.* 46, 14–22. doi: 10.1021/ar300009f

Eom, N., Cho, H. B., Song, Y., Lee, W., Sekino, T., and Choa, Y. H. (2017). Room-Temperature H2 gas sensing characterization of graphene-doped porous silicon via a facile solution dropping method. *Sensors* 17:2750. doi: 10.3390/s17122750

Hagfeldt, A., Boschloo, G., Sun, L. C., Kloo, L., and Pettersson, H. (2010). Dye-sensitized solar cells. *Chem. Rev.* 110, 6595–6663. doi: 10.1021/cr900356p

Hernandez, Y., Nicolosi, V., Lotya, M., Blighe, F. M., Sun, Z., De, S., et al. (2008). High-yield production of graphene by liquid-phase exfoliation of graphite. *Nat. Nanotechnol.* 3, 563–568. doi: 10.1038/nnano.2008.215

Kim, H. W., Na, H. G., Kwon, Y. J., Kang, S. Y., Choi, M. S., Bang, J. H., et al. (2017). Microwave-Assisted synthesis of graphene–SnO$_2$ Nanocomposites and their applications in gas sensors. *ACS Appl. Mater. Interf.* 9, 31667–31682. doi: 10.1021/acsami.7b02533

Liu, X., Ning, H., Chen, W., Fang, Z., Yao, R., Wang, X., et al. (2018). Effect of Source/Drain Electrodes on the Electrical Properties of Silicon-Tin Oxide Thin-Film Transistors. *Nanomaterials* 8, 293–300. doi: 10.3390/nano8050293

Long, H., Zeng, W., Wang, H., Qian, M., Liang, Y., and Wang, Z. (2018). Self-Assembled Biomolecular 1D Nanostructures for Aqueous Sodium-Ion Battery. *Adv. Sci.* 5, 1700634–1700637. doi: 10.1002/advs.201700634

Narjinary, M., Rana, P., Sen, A., and Pal, M. (2017). Enhanced and selective acetone sensing properties of SnO$_2$-MWCNT nanocomposites: Promising materials for diabetes sensor. *Mater. Des.* 115, 158–164. doi: 10.1016/j.matdes.2016.11.042

Nemade, K. R., and Waghuley, S. A. (2013). Chemiresistive Gas Sensing by Few-Layered Graphene. *J. Electron. Mater.* 42, 2857–2866. doi: 10.1007/s11664-013-2699-4

Neri, G., Leonardi, S. G., Latino, M., Donato, N., Baek, S., Conte, D. E., et al. (2013). Sensing behavior of SnO$_2$/reduced graphene oxide nanocomposites toward NO$_2$. *Sens. Actuators B* 179, 61–68. doi: 10.1016/j.snb.2012.10.031

Praus, L., Svoboda, L., Dvorský, R., and Reli, M. (2018). Nanocomposites of SnO$_2$ and g-C$_3$N$_4$: preparation, characterization and photocatalysis under visible LED irradiation. *Ceram. Int.* 44, 3837–3846. doi: 10.1016/j.ceramint.2017.11.170

Satoh, K., Murakami, S., Kanaoka, Y., Yoshiharu, Y., Kakehi, Y., Sakurai, Y., et al. (2018). Effect of postannealing on properties of ZnO-SnO$_2$ thin film transistors. *J. Vac. Sci. Technol. A* 36:02C105. doi: 10.1116/1.5003283

Shi, Y., Ma, D., Wang, W., Zhang, L., and Xu, X. (2017). A supramolecular self-assembly hydrogel binder enables enhanced cycling of SnO$_2$-based anode for high-performance lithium-ion batteries. *J. Mater. Sci.* 52, 3545–3555. doi: 10.1007/s10853-016-0623-z

Thu, N. T. A., Cuong, N. D., Le, C. N., Khieu, D. Q., Nam, P. C., Toan, N. V., et al. (2018). Fe$_2$O$_3$ nanoporous network fabricated from Fe$_3$O$_4$/reduced

graphene oxide for high-performance ethanol gas sensor. *Sens. Actuators B* 255, 3275–3283. doi: 10.1016/j.snb.2017.09.154

Xu, S., Zhao, H., Xu, Y., Xu, R., and Lei, Y. (2018). Carrier Mobility-Dominated Gas Sensing: A Room-Temperature Gas-Sensing Mode for SnO$_2$ Nanorod Array Sensors. *ACS Appl. Mater. Interfaces.* 10, 13895–13902. doi: 10.1021/acsami.8b03953

Yan, H., Song, P., Zhang, S., Yang, Z., and Wang, Q. (2015). Dispersed SnO$_2$ nanoparticles on MoS$_2$ nanosheets for superior gas-sensing performances to ethanol. *RSC Adv.* 5, 79593–79599. doi: 10.1039/C5RA15019A

Yoon, H. J., Jun, D. H., Yang, J. H., Zhou, Z., Yang, S. S., and Cheng, M. C. (2012). Carbon dioxide gas sensor using a graphene sheet. *Sens. Actuators B* 157, 310–313. doi: 10.1016/j.snb.2011.03.035

Zhang, M., Liu, L., He, T., Wu, G., and Chen, P. (2016). Melamine assisted solid exfoliation approach for the synthesis of few-layered fluorinated graphene nanosheets. *Mater. Lett.* 171, 191–194. doi: 10.1016/j.matlet.2016.02.042

Zhang, S. S., Sun, G., Li, Y., Zhang, B., Lin, L., Wang, Y., et al. (2018). Continuously improved gas-sensing performance of SnO$_2$/Zn$_2$SnO$_4$ porous cubes by structure evolution and further NiO decoration. *Sens. Actuators B* 255, 2936–2943. doi: 10.1016/j.snb.2017.09.114

Zhang, Y. J., Zeng, W., and Lin, Y. Q. (2018). Hydrothermal synthesis and controlled growth of hierarchical 3D flower-like MoS$_2$ nanospheres assisted with CTAB and their NO$_2$ gas sensing properties. *Appl. Surf. Sci.* 455, 276–282. doi: 10.1016/j.apsusc.2018.05.224

Zhao, K., Zhang, L., Xia, R., Dong, Y., Xu, W., Niu, C., et al. (2016). SnO$_2$ Quantum Dots@Graphene Oxide as a High-Rate and Long-Life Anode Material for Lithium-Ion Batteries. *Small* 2, 588–594. doi: 10.1002/smll.201502183